

Measured group birefringence and group velocity dispersion of elliptical-core ZBLAN fibres for mid-infrared supercontinuum generation

Shreesha Rao D. S.^{1,2,*}, Christian R. Petersen^{1,3}, Anupamaa Rampur², Ole Bang^{1,3}, and Alexander M. Heidt²

¹DTU Electro, Department of Electrical and Photonics Engineering, Technical University of Denmark, Ørsted Plads, 2800 Kongens Lyngby, Denmark

²Institute of Applied Physics, University of Bern, Sidlerstrasse 5, 3012 Bern, Switzerland.

³NORBLIS ApS, Virumgade 35D, 2830 Virum, Denmark.

*corresponding author: Shreesha Rao D. S. (shdes@dtu.dk)

ABSTRACT

Polarisation-maintaining ZBLAN optical fibres with small elliptical cores are attractive for nonlinear frequency conversion, for example in supercontinuum generation (SCG), and for dispersion management in ultrafast fibre laser systems operating in the mid-infrared (MIR) spectral region. Accurate characterisation of group birefringence and group velocity dispersion (GVD) is essential for modelling ultrafast pulse propagation in such fibres, yet experimental data remain scarce. Here, we present broadband measurements of group birefringence and GVD in four elliptical-core ZBLAN fibres, selected for their potential for low-noise MIR SCG, over the wavelength range 1.4 to 4.3 μm . Using polarisation-resolved white-light spectral interferometry, we quantify the dispersion characteristics of both fundamental modes in each fibre. Measurement uncertainties are evaluated using a standard deviation analysis to ensure reliability. This work aims to support the development of MIR supercontinuum sources and to facilitate the understanding of nonlinear optical phenomena in ZBLAN fibres.

Background & summary

Optical fibres are critical components in modern science and technology, serving applications such as telecommunications, environmental sensing, and laser systems. Their performance depends on the ability to accurately control both linear and nonlinear light propagation, which in turn depends on the optical properties of the fibre. Accurate modelling of pulse propagation is essential to predict how light interacts with the waveguide structure and material dispersion. Such modelling not only provides insight into the underlying physics but also enables accurate design and fabrication of fibres to achieve desired characteristics for specific applications.

Optical fibres are waveguides made of a core and cladding, designed to confine and guide light. The refractive index of the core material is denoted n_{core} , and that of the cladding as n_{clad} . Fibres can be engineered to support only the fundamental mode for frequencies lower than a certain cut-off frequency. In addition, some fibres can be designed to be endlessly single mode. The modes that propagate in the fibre experience an effective refractive index $n_{\text{eff}}(\omega)$, which depends on frequency and accounts for the waveguide structure and material properties. The propagation constant, $\beta(\omega)$, is related to $n_{\text{eff}}(\omega)$ as $\beta(\omega) = n_{\text{eff}}(\omega) \cdot \omega/c$, where ω is the angular frequency of light, and c is the speed of light in vacuum. The first derivative of the propagation constant, $\beta_1(\omega) = d\beta/d\omega$, gives the group velocity v_g of an optical pulse, with $v_g = 1/\beta_1(\omega)$. The second derivative, $\beta_2(\omega) = d^2\beta/d\omega^2$, is the group velocity dispersion (GVD), a critical parameter that determines the extent to which different frequency components of a pulse spread temporally as they propagate. Group velocity dispersion, $\beta_2(\omega)$, is typically expressed in units of ps^2/km . Another commonly used group velocity dispersion parameter is D , which is defined as the derivative of $\beta_1(\omega)$ with respect to wavelength, λ , and is usually expressed in units of $\text{ps}/(\text{km}\cdot\text{nm})$. The relation between the two group velocity dispersion parameters is given by $D = -2\pi c \cdot \beta_2 / \lambda^2$.

The GVD determines how the pulse evolves during propagation. It is a key linear effect that influences pulse propagation in the fibre. As the pulse propagates through the fibre, its constituent frequency components can become temporally separated due to differences in their propagation speeds. This frequency variation across the pulse duration is referred to as chirp. If the intensity of the pulse travelling through the fibre is high enough, nonlinear effects may arise. The pulse then experiences an interplay between linear, and nonlinear effects. One such nonlinear effect is self-phase modulation (SPM), which occurs when the refractive index experienced by the pulse depends on its intensity. As the intensity of the pulse varies along its duration, the

pulse experiences a nonlinear refractive index change over the pulse duration, leading to the generation of new frequencies. As a result, SPM can induce a chirp across the pulse due to this nonlinearity. In the special case where the nonlinear chirp from SPM, and the linear chirp from GVD counteract each other, the pulse can evolve into a stable state which maintains its spectral and temporal profile during further propagation. Such pulses, which preserve their spectro-temporal characteristics over long distances due to a precise balance between dispersive and nonlinear effects, are known as solitons. The pulse propagation in the fibre can be modelled using the generalised nonlinear Schrödinger equation (GNLSE)^{1,2}. This equation accounts for both the linear and nonlinear effects influencing pulse evolution in the fibre. A key parameter in implementing the GNLSE is the wavelength-dependent GVD profile of the fibre, which must be precisely known for accurate modelling of pulse evolution.

GVD measurement across a broad wavelength region is particularly important in studies of supercontinuum generation (SCG) in fibres. SCG is an extreme nonlinear process which leads to a spectrally broad output in a medium, when pumped by a relatively narrow-band input pulse. In a traditional SC source, a nanosecond (ns) or a picosecond (ps) pump with a central wavelength slightly longer than the fibre's zero-dispersion wavelength (ZDW) is launched into the fibre. The spectrum primarily broadens through modulation instability, which leads to soliton formation in the anomalous dispersion regime and the generation of associated dispersive waves in the normal dispersion regime³. These dispersive waves contribute significantly to the spectral extension of the SC. The wavelength range at which dispersive waves are generated can be accurately modelled when the fibre's GVD is known across the entire spectral regime covered by the SC. With high-power ns and ps lasers around 1 μm , and silica fibres whose ZDW lies below the pump wavelength, SC spanning 390–2400 nm can be achieved⁴. This range covers the full transmission window of silica fibres. The ability to model and optimise such broad spectra depends critically on accurate measurements of GVD across the entire bandwidth. These multi-octave-spanning sources have been used in confocal fluorescence microscopy^{5,6}, among other applications.

A major drawback of such SC sources is their high pulse-to-pulse fluctuations⁷. This is inherent to the fundamental mechanism driving SCG. Since modulation instability is seeded by noise, the temporal and spectral profiles can vary significantly from pulse-to-pulse, even when the pump pulse characteristics remain unchanged⁸. One way to overcome this limitation is to generate the SC entirely in the normal dispersion regime of the fibre⁹. When a femtosecond (fs) pulse is launched into the fibre in the normal dispersion regime, coherent SPM and optical wave breaking (OWB) can produce an ultra-low-noise SC¹⁰, provided the entire generated spectrum remains within the normal dispersion regime¹¹. Such an SC can maintain a single pulse in the time domain and a flat, smooth spectral profile⁹.

A single-mode fibre can support two fundamental modes that correspond to orthogonal polarisation states. In a low-birefringence fibre, these two orthogonal modes have very similar characteristics; for example, their group velocities can be nearly identical. As the low-birefringence results in similar propagation constants for the two modes, light can couple between them during propagation. As the group velocities of these modes are similar over a broad wavelength range, power in one mode can noise-seed the spectrum in the other, leading to polarisation mode instability (PMI) – a nonlinear coupling phenomenon causing power transfer between polarisation modes. Since the spectra resulting from PMI are noise-seeded, the resulting SC can exhibit high pulse-to-pulse fluctuation¹², despite being in the normal dispersion regime. By incorporating stress rods in the cladding, shaping the core elliptically, combining both methods, or by using other methods, for example, by structuring the cladding near the core to break symmetry, the phase birefringence of the fibre can be increased. This ensures that the propagation constants of the two polarisation modes are sufficiently separated; these fibres are known as polarisation-maintaining (PM) fibres. While phase birefringence determines the separation in propagation constants between the two modes, PM fibres require sufficiently high group birefringence to effectively suppress PMI. In fibres with high group birefringence, the large difference in group velocities prevents coupling between the polarisation modes¹³. Using such PM fibres with a normal dispersion profile enables the generation of ultra-low-noise SC^{12,14}, which is essential for applications requiring high sensitivity in detection.

Ultra-low-noise SC sources, exhibiting relative-intensity noise (RIN) levels comparable to those of technologically mature ultra-low-noise fs pump sources at 1.0 μm ¹⁵ and 1.55 μm ¹⁶, have been demonstrated in silica-based fibres. However, their spectral extension has typically been limited to the near-infrared (NIR), up to approximately 2.4 μm , due to the high loss in silica fibres at longer wavelengths. These SC sources enable a number of applications in the NIR such as high-quality pulse compression¹⁷, single-beam coherent anti-Stokes Raman spectroscopy¹⁸, ultra-high resolution (UHR) spectral-domain optical coherence tomography (OCT)¹⁹, UHR apertureless scanning near-field optical microscopy²⁰ (SNOM), and dual-comb spectroscopy²¹.

Extending SCG into the mid-infrared (MIR) region is highly desirable for a number of applications, for example in spectral-domain OCT²². In spectral-domain OCT, penetration depth is limited when using NIR sources due to scattering losses, which for small particles scale approximately as λ^{-4} . As scattering decreases rapidly with increasing wavelength in this regime, using a MIR source can significantly increase penetration depth. Fluoride fibres are excellent candidates to extend SCG into the MIR due to their broad transmission window, which spans from below 300 nm to beyond 4.5 μm , thereby covering the visible, NIR, and a part of MIR regions. Among these, one of the fibres that are commercially available is made from ZBLAN

(ZrF₄–BaF₂–LaF₃–AlF₃–NaF). To date, SCG in ZBLAN fibres has been demonstrated by pumping in the anomalous dispersion regime^{23,24}, and its applications are beginning to be explored using such sources²². An SC spanning this MIR region also covers important gas absorption features, including carbon monoxide²⁵, methane²⁶, ammonia²⁷, and other molecules, making it highly relevant for spectroscopy and sensing. However, measured dispersion data for ZBLAN fibres remain scarce, limiting accurate modelling and optimisation of SC sources. Furthermore, SCG in normal-dispersion fluoride fibres has not yet been studied, largely due to the lack of fibres with such dispersion profiles. Ultra-low-noise SCG in PM-ZBLAN fibres with tailored normal dispersion is needed for a range of applications; for instance, it could significantly improve the sensitivity of MIR OCT systems^{19,22} and enable SNOM in the MIR, which is yet to be realised because suitable ultra-low-noise sources are not available.

Item name	Fibre core/cladding [μm]	Numerical aperture
ZEF-2.2×5.5/125-N	5.5 × 2.4/123	0.23 ± 0.02 at 1.20 μm
ZEF-2.7×6.7 /95×125-N	6.7 × 2.7/124 × 96	0.26 ± 0.02 at 1.24 μm
ZEF-4.5×9/125-N	8.9 × 4.1/121	0.20 ± 0.02 at 0.84 μm
ZEF-6×10/125-N	10.6 × 5.6/121	0.20 ± 0.02 at 0.84 μm

Table 1. Core and cladding dimensions, along with numerical aperture values at specified wavelengths, for the elliptical core PM-ZBLAN fibres used in this study. These details are taken from the datasheets provided by the fibre manufacturer, FiberLabs Inc., Japan.

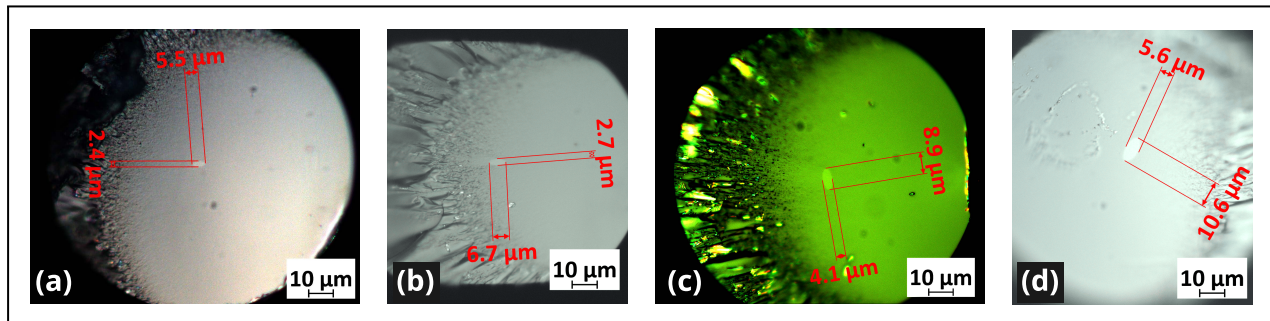


Fig. 1. 100× magnified cross-sections of the four elliptical-core fibres.

In this work, four fibres were selected to represent a realistic and practically relevant subset of commercially available elliptical-core PM-ZBLAN fibres. The cross-sections of the four fibres are shown in Fig. 1(a)–(d). The core dimensions span from 5.5 × 2.4 μm to 10.6 × 5.6 μm. The core and cladding dimensions of the fibres are provided in Table 1, along with the numerical aperture values at specified wavelengths. These details are taken from the datasheets provided by the fibre manufacturer, FiberLabs Inc., Japan. The core dimensions are used to refer to the individual fibres. By providing broadband measurements of both group birefringence and GVD for the two fundamental modes of each fibre, this work fills an important gap in the literature. The wavelength range covered, 1.4 to 4.3 μm, encompasses the majority of the low-loss transmission region of ZBLAN and extends well beyond the range normally accessible using conventional white-light interferometry, which is typically limited to the transmission window of silica fibres.

As the measurements use fibres that are available off-the-shelf, the dataset serves not only as a reference for the scientific community but also as a practical resource for researchers seeking to model or optimise MIR nonlinear propagation. The elevated group birefringence achievable in these fibres suppresses PMI over a broad spectral range, thereby enabling the generation of ultra-low-noise SC entirely within the normal dispersion regime. The range of core dimensions studied encompasses PM-ZBLAN fibres with ZDW shorter than 2 μm to longer than 3.75 μm. In addition to their relevance for MIR ultra-low-noise SC sources based on PM-ZBLAN fibres—a capability that has not yet been fully demonstrated—accurate knowledge of the dispersion and group birefringence of these fibres is valuable for a broad range of applications such as third-harmonic generation²⁸ and dispersion management in 2.8 μm laser systems²⁹. The data provided in this paper are intended to support reproducible modelling, reduce uncertainty in numerical studies, and facilitate the development of next-generation MIR fibre sources.

Methods

The fibres were cleaved using a Vytron cleaver (Thorlabs: CAC4020AFJ) with a tension of ~ 100 g. The intended fibre length after cleaving was approximately 20 cm. After cleaving the input and output ends, the actual length of each fibre was measured using a ruler with an accuracy of ± 1 mm. The fibres were mounted with the input end held in a keyway bare fibre holder placed on a three-axis translation stage, and the output end secured in a keyway bare fibre rotation mount on a separate three-axis translation stage. The sequence of measurements was as follows: (i) identification of the principal axes of the fibre, (ii) broadband measurement of the group birefringence, and (iii) broadband measurement of the GVD.

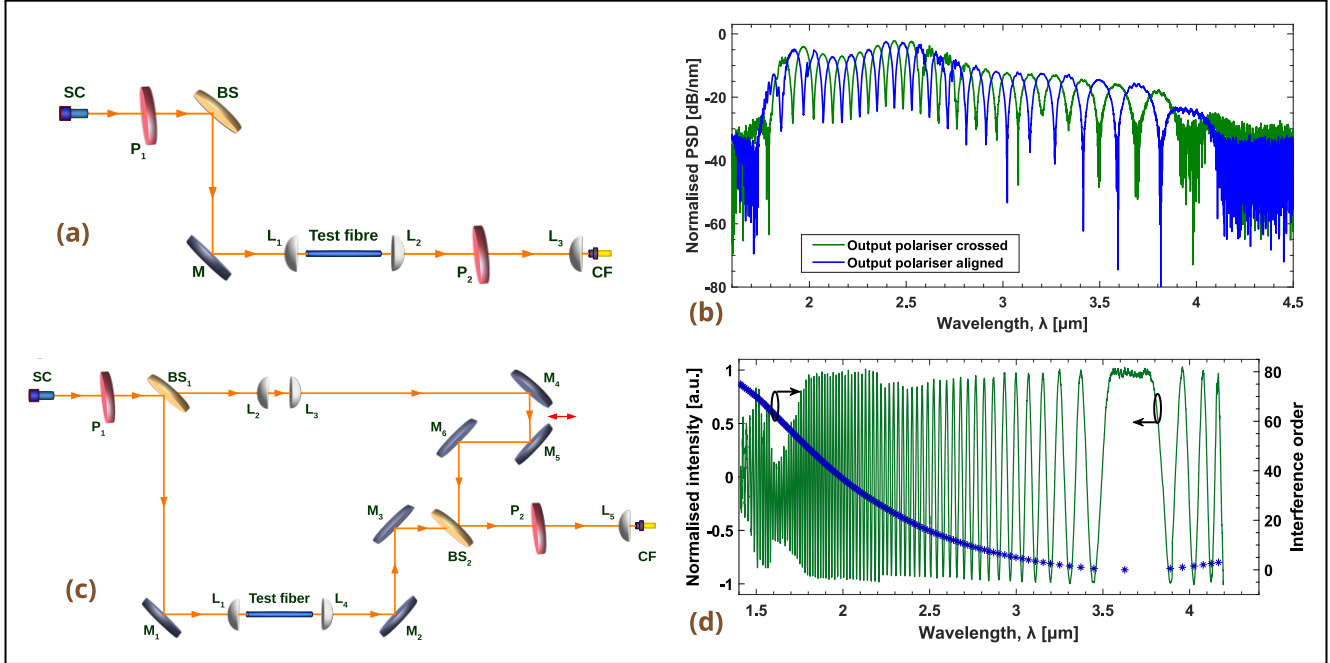


Fig. 2. (a) Schematic of the group birefringence measurement setup. (b) Example interference spectra for the group birefringence measurement, with the output polariser crossed in green and aligned in blue relative to the input polariser. (c) Schematic of the white light spectral interferometry setup used for GVD measurement. (d) Example spectral interference pattern I_{Interf} , for the GVD measurement showing fringes around the phase-matching point in green. The corresponding fringe order for this measurement is shown in blue with respect to the right y-axis

Measurement of group birefringence

A source (NKT Photonics: SuperK MiR 15) covering the wavelength range 1.4–4.3 μm was used. The source spectrum exhibits a peak at 1.55 μm corresponding to the SC pump, and a dip around 1.7 μm . The group birefringence measurement setup is shown in Fig. 2(a). For this measurement, only the reflected beam from the beam splitter (BS, Thorlabs: BSW511) was used. Light was coupled into the fibre using an aspherical lens L₁, and the output light was collimated with an aspherical lens L₂.

The angular separation between the two fundamental modes of the fibre is typically 90°, although their orientation may vary slightly between fibres due to structural asymmetries. To identify the angle of the transmission axis of the input polariser at which light is coupled into a given principal axis of the fibre, the transmission axis of the input polariser (P₁, Thorlabs: LPMIR050-MP2) was set to an arbitrary initial angle, say 0°. Hereafter, ‘rotating the polariser’ refers to rotating its transmission axis. At the start of the measurement, the output polariser (P₂, Thorlabs: LPMIR050-MP2) was rotated to locate the minimum transmitted power, and the corresponding angle, $\theta_{2,\text{min}}$, was recorded; P₂ was then rotated to locate the maximum, and the angle $\theta_{2,\text{max}}$ was recorded. At these angles, the transmitted power was measured.

The measurement proceeded by rotating P₁ in 10° steps; at each angle, the transmitted power through P₂ was recorded twice: first with P₂ set to $\theta_{2,\text{min}}$, then with it set to $\theta_{2,\text{max}}$. As P₁ was rotated through 360°, each of the two traces varied near-sinusoidally with two maxima and two minima. The traces were complementary, with maxima and minima interchanged. The angles of P₁ at which the extrema occurred indicated the orientations that coupled light into one fundamental mode and into the orthogonal mode, respectively. While either trace alone would suffice to find the extrema, both complementary traces were

recorded at every angle to reduce any ambiguity when identifying the angles associated with coupling to the fibre's fundamental modes.

After the orientations of the two principal axes were determined, the input polariser P_1 was rotated such that equal power was coupled into both orthogonal fundamental modes of the fibre. When the angular separation between the maxima and the adjacent minima is 90° , equal power can be coupled into the two fundamental modes by aligning P_1 at an angle of 45° to the principal axes. The light then passed through P_2 and was coupled to a collection fibre (CF, Thorlabs: P1-23Z-FC-1) using an aspherical lens (L_3 , Thorlabs: C036TME-D), as shown in Fig. 2(a). The collection fibre was then connected to a broadband optical spectrum analyser (Instrument Systems: Spectro 320), capable of recording spectra in the wavelength range $0.18\text{--}5.0\ \mu\text{m}$.

The spectra were recorded with the output polariser crossed^{30,31} and then aligned with respect to the input polariser. As the input polariser was set at 45° relative to the angles that excite the two fundamental modes of the fibre, both modes were excited equally. In both configurations, interference patterns were observed. The two spectra differ in that the positions of the maxima and minima are interchanged when comparing the crossed-polariser method to the aligned-polariser method. Example interference spectra with the output polariser crossed plotted in green and aligned plotted in blue relative to the input polariser are shown in Fig. 2(b).

Group birefringence, B_g , depends on the fringe spacing in the measured spectral interference patterns. The fringe spacing, $\Delta\lambda$, is the wavelength difference between adjacent peaks in the spectral interference pattern. The corresponding wavelength for each calculated value of B_g can be taken as the centre wavelength between the adjacent peaks. The group birefringence as a function of wavelength can be calculated using:

$$B_g(\lambda) = \frac{1}{L_f} \cdot \frac{\lambda^2}{\Delta\lambda}, \quad (1)$$

where L_f is the length of the test fibre. We measured group birefringence of the four elliptical-core fibres. For each fibre, two sets of measurements were performed: one with the output polariser crossed with respect to the input polariser, and the other with the output polariser angled relative to the input polariser.

Measurement of group velocity dispersion

Broadband dispersion measurements of the elliptical-core PM-ZBLAN fibres were performed using white-light spectral interferometry. The GVD measurement method is based on the approach presented in a previous studies^{32,33}. The experimental setup used for the GVD measurement is shown in Fig. 2(c) and is based on a Mach–Zehnder interferometer. After passing through the polariser (P_1 , Thorlabs: LPMIR050-MP2), the light is split into two paths by a beam splitter (BS_1 , Thorlabs: BSW511). The reflected part of the light is directed to the test arm of the interferometer, while the transmitted part enters the reference arm. In the test arm, a mirror M_1 directs the beam to an aspherical lens L_1 , which couples the light into the fibre under test. The output from the fibre is collimated using an aspherical lens L_4 , and the beam is then directed by mirrors M_2 and M_3 , through the beam splitter (BS_2 , Thorlabs: BSW511) and a second polariser (P_2 , Thorlabs: LPMIR050-MP2). Finally, the light is coupled into the collection fibre (CF, Thorlabs: P1-23Z-FC-1) using an aspherical lens (L_5 , Thorlabs: C036TME-D).

In the reference arm, light transmitted through the beam splitter BS_1 is focused using an aspherical lens L_2 , which is identical to lens L_1 . The beam is then collimated using lens L_3 , which is identical to lens L_4 . The collimated light is directed by mirrors M_4 , M_5 , and M_6 to a second beam splitter BS_2 . The part of the light reflected from BS_2 passes through the polariser P_2 and is also coupled into the collection fibre using an aspherical lens L_5 . Mirrors M_4 and M_5 are mounted on a one-dimensional translation stage, allowing the optical path length in the reference arm to be varied. This variable path length is indicated by the bidirectional arrow in Fig. 2(c). The setup is designed so that light in both the reference and test arms interacts with identical optical components, except for the fibre in the test arm. As a result, any difference in the properties of the light travelling through the two arms arises solely from the fibre under test. All mirrors used in the setup were silver mirrors (M_i , Thorlabs: PF10-03-P01), and all lenses were aspheric. The spectra from the collection fibre were measured using an optical spectrum analyser (Instrument Systems: Spectro 320).

To measure the dispersion of one of the fundamental modes of the fibre, polariser P_1 was rotated to selectively couple light into a single fundamental mode. Polariser P_2 was then aligned to transmit light corresponding to that same mode, thereby suppressing any residual light coupled into the orthogonal mode. When light from both arms is present in the measured spectrum, the optical path length in the reference arm can be adjusted using mirrors M_4 and M_5 mounted on a one-dimensional translation stage. This enables the optical path lengths in both the fibre arm and the reference arm to be made equal for a given wavelength. At this wavelength, the light accumulates the same phase in both arms; this wavelength region is referred to as the phase-matching point. Spectral interference fringes appear on either side of this point. An example of such a spectral interference pattern is shown in Fig. 2(d) in green, plotted with respect to the left y-axis. The phase-matching point occurs around $3.7\ \mu\text{m}$. Due to a significant dip in the SC source around $1.7\ \mu\text{m}$, the fringe visibility is low in that region, as it was not possible to couple equal amounts of light into both the fibre and reference arms.

To obtain the interference pattern shown in Fig. 2(d), the spectrum was first measured with light from both arms present simultaneously, denoted as I_{Total} . Spectra were then recorded from each arm individually while the other was blocked. The intensities from the individual arms were subtracted from I_{Total} , and the result was normalised to yield the spectral interference pattern I_{Interf} . The resulting interference fringes were then numbered, with the fringe number denoted by i , updated by 1 for each adjacent fringe maximum. When the numbering reaches the phase-matching point, the direction of numbering was reversed. The fringe order of the example interference pattern, I_{Interf} , shown in Fig. 2(d), is plotted in blue with respect to the right y-axis. The fringe order is then fitted to the equation:

$$i = a_1\lambda^{-5} + a_2\lambda^{-3} + a_3\lambda^{-1} + a_4\lambda^1 + a_5\lambda^3 - m, \quad (2)$$

where, $a_1 = -A_1 L_f$, $a_2 = -A_2 L_f$, $a_3 = -A_4 L_f$, $a_5 = -A_5 L_f$, and m is an integer. The expression for the fringe order i , given in Eq. (2), is derived from the modified Cauchy equation for the refractive index. From the fit, the ‘a’-coefficients are obtained and subsequently converted to the ‘A’-coefficients. Using these A-coefficients, the measured GVD as a function of wavelength can be obtained. The group velocity dispersion D is given by:

$$D = -\frac{1}{c} [20A_1\lambda^{-5} + 6A_2\lambda^{-3} + 2A_4\lambda + 12A_5\lambda^3]. \quad (3)$$

GVD measurements were repeated three times for each polarisation mode, with the phase-matching point varied across the measurements. Note that the beam splitter shown in Fig. 2(a) was not required for the group birefringence measurements but was included from the outset to enable a seamless transition to the GVD measurements. The reflected light from the beam splitter was used for the group birefringence measurements. This approach avoided disturbing the fibre alignment when reconfiguring the setup from group birefringence to GVD measurements.

Data records

The mean group birefringence obtained from the cross and aligned polariser measurements for each fibre is plotted in blue in Fig. 3(a)–(d). The wavelength versus mean group birefringence values is available through Figshare³⁴. The A-coefficient for each mode of the four fibres listed in Table 2, and plotted in blue in Figs. 3(e)–(h), corresponds to one of the three measurements rather than the mean of the three measurements. This is done because the GVD obtained from an individual measurement is a smooth curve, unlike the mean of the three measurements. The smooth curves can then be integrated or differentiated if needed. The GVD of both fundamental modes of each fibre was measured. The mode with the lower absolute value of GVD at

Fibre [μm]	Mode	A ₁	A ₂	A ₄	A ₅	Measurement range
5.5 × 2.4	Mode I	504.245	131.132	4740.566	-86.368	1.460–2.810 μm
	Mode II	-1037.736	3270.755	4125.000	-74.764	
6.7 × 2.7	Mode I	6717.172	-9969.697	3406.566	-38.449	1.400–4.210 μm
	Mode II	3964.646	-6121.212	3251.010	-37.763	
8.9 × 4.1	Mode I	4013.333	-5323.810	1703.810	-25.133	1.420–4.050 μm
	Mode II	4581.905	-5990.476	1798.095	-26.562	
10.6 × 5.6	Mode I	3739.196	-4276.382	318.492	-5.945	1.400–4.340 μm
	Mode II	4978.392	-5954.774	484.573	-7.884	

Table 2. A-coefficients to obtain the measured group velocity dispersion D for mode I and mode II of each elliptical-core PM-ZBLAN fibre. The measurement range indicates the wavelength interval over which spectral interference fringes were measured.

2 μm was designated as mode I, and the orthogonal mode was designated as mode II. The A-coefficients used to calculate the GVD for mode I and mode II of each fibre are provided in the Table 2. These coefficients correspond to one of the three measurements performed for each mode. The GVD for this selected measurement of mode I in the four fibres is plotted in Figs. 3(e)–(h) in blue. Since the fit to the fringe order was performed with wavelength in μm, the variable λ in Eq. (3) must also be expressed in μm, while the speed of light is expressed in m/s. Table 2 also lists the measurement ranges, which indicate the wavelength range over which the interference fringes were measured. Using Eq. (3), the GVD can also be estimated outside,

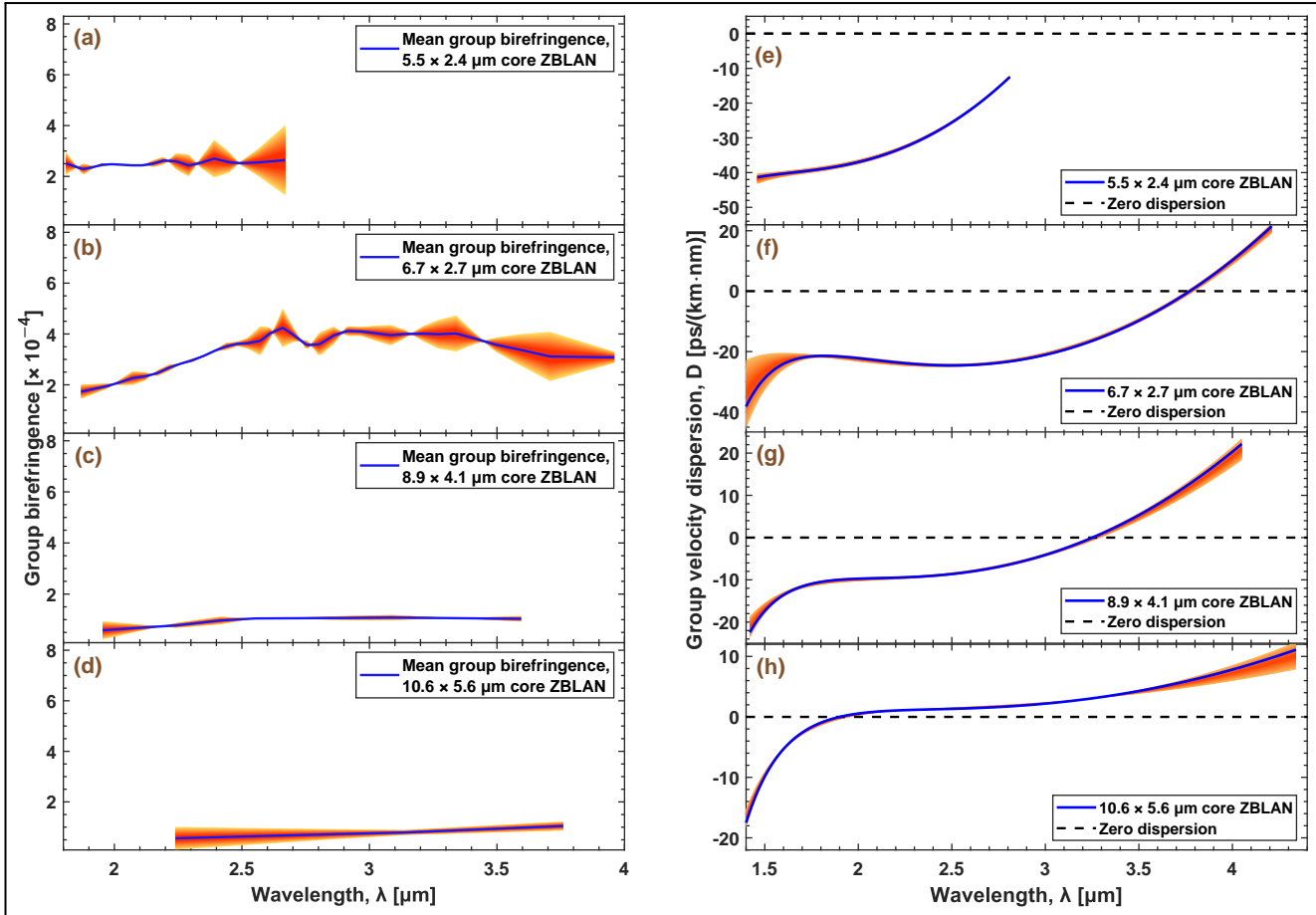


Fig. 3. (a)–(d) Mean group birefringence values in blue for the four elliptical-core PM-ZBLAN fibres, along with the $\pm 2 \times$ standard deviation error band shown in shades of orange. (e)–(h) Group velocity dispersion D curves for mode I of the four elliptical-core PM-ZBLAN fibres, along with the $\pm 4 \times$ standard deviation error band shown in shades of orange. Blue curves correspond to one of the three independent measurements conducted for each fibre. The dashed black line indicates zero dispersion.

but close to, this range with reasonable accuracy. The derivation of the modified Cauchy equation is available in the referenced work³⁵ and further detailed in supplementary material A.

The GVD of the $5.5 \times 2.4 \mu\text{m}$ core fibre is normal across the entire wavelength range of the measurement. It was not possible to couple light at wavelengths longer than $2.81 \mu\text{m}$ for this fibre in our setup. The $6.7 \times 2.7 \mu\text{m}$ core fibre has a ZDW at $3.772 \mu\text{m}$, the $8.9 \times 4.1 \mu\text{m}$ core fibre has a ZDW at $3.252 \mu\text{m}$, and the $10.6 \times 5.6 \mu\text{m}$ core fibre has a ZDW at $1.9 \mu\text{m}$. These ZDWs correspond to mode I of the measurements plotted in blue in Figs. 3(e)–(h).

In this work, we have presented experimentally measured broadband values of group birefringence and GVD for elliptical core PM-ZBLAN fibres. The measured GVD can be compared with earlier simulation-based studies, such as those on circular core ZBLAN fibres³⁶. Our results demonstrate what is practically achievable in terms of GVD in elliptical-core PM-ZBLAN fibres. We believe that the measured group birefringence and GVD will be useful both for planning experiments involving these fibres and for modelling the results of experiments carried out using them. The GVD, which can be obtained by substituting the A-coefficients provided in Table 2 into Eq. (3) for both fundamental modes of the four elliptical-core PM-ZBLAN fibres, is also available through Figshare³⁴.

Technical validation

The experimental methods for measuring group birefringence and GVD are based on earlier studies and represent well-established techniques that have been widely employed for group birefringence³⁷ and GVD^{14,38} measurements in the NIR, including for PM fibres. Similar experimental setups have been used to measure GVD in the 1.3 – $4.5 \mu\text{m}$ range in chalcogenide

fibres³⁹ and in waveguides on gallium lanthanum sulphide⁴⁰. To quantify the experimental uncertainty, an error analysis was carried out for both the group birefringence and GVD measurements.

Calculation of error

The total uncertainty in the group birefringence measurements was calculated by combining two independent sources of error using the root-sum-of-squares method: experimental variability and the systematic uncertainty in the fibre length. For each fibre, two separate measurements were performed using complementary techniques—one with the transmission axis of the output polariser crossed relative to the input polariser, and the other with the two polarisers aligned. The two resulting datasets were interpolated to a common wavelength grid, which enabled a direct point-by-point calculation of the mean group birefringence and the standard deviation between the two measurements.

Fibre core [μm]	[Mean group birefringence $\pm 2 \times$ standard deviations] $\times 10^{-4}$		
	at 2.00 μm	at 2.40 μm	at 2.80 μm
5.5 \times 2.4	2.47 \pm 0.03	2.68 \pm 0.69	—
6.7 \times 2.7	2.03 \pm 0.02	3.37 \pm 0.04	3.59 \pm 0.42
8.9 \times 4.1	0.62 \pm 0.28	0.95 \pm 0.15	1.06 \pm 0.05
10.6 \times 5.6	—	0.60 \pm 0.38	0.71 \pm 0.22

Table 3. Mean group birefringence values for the four elliptical-core PM-ZBLAN fibres at selected wavelengths, with their corresponding measurement error $\pm 2 \times$ standard deviation.

In addition to this experimental uncertainty, the systematic error from the measured fibre length was also included. An uncertainty of ± 1 mm in the fibre length was taken into account to calculate the corresponding proportional uncertainty in the group birefringence. This length-dependent error was then combined with the standard deviation from the two independent measurements using a root-sum-of-squares method. This combination yields a total uncertainty that quantifies the errors in the measurement.

The mean group birefringence for the four elliptical-core PM-ZBLAN fibres is shown in blue in Fig. 3(a)–(d), with the associated error band shown in shades of orange. The error band represents ± 2 times the standard deviation. The group birefringence values obtained from the cross-polariser and aligned-polariser methods intersect at certain wavelengths, which leads to reduced measurement error at those wavelengths. The mean group birefringence at selected wavelengths for the fibres is provided in Table 3, with a corresponding measurement error of $\pm 2 \times$ standard deviation.

Fibre core [μm]	Mode	[Mean GVD $\pm 4 \times$ standard deviations] [ps/(km·nm)]			
		at 1.55 μm	at 2.00 μm	at 2.80 μm	at 4.00 μm
5.5 \times 2.4	Mode I	−40.81 \pm 1.01	−36.93 \pm 0.70	−12.96 \pm 0.37	—
	Mode II	−40.05 \pm 5.28	−37.43 \pm 0.96	−13.73 \pm 3.70	—
6.7 \times 2.7	Mode I	−24.71 \pm 4.19	−22.49 \pm 0.86	−23.21 \pm 0.57	+09.90 \pm 1.26
	Mode II	−23.79 \pm 1.87	−24.48 \pm 0.71	−23.45 \pm 0.51	+11.33 \pm 0.96
8.9 \times 4.1	Mode I	−14.89 \pm 0.88	−09.90 \pm 0.45	−06.41 \pm 0.39	+19.15 \pm 2.41
	Mode II	−14.79 \pm 5.80	−10.14 \pm 0.45	−06.45 \pm 0.42	+20.50 \pm 3.21
10.6 \times 5.6	Mode I	−07.19 \pm 0.31	+00.45 \pm 0.24	+01.82 \pm 0.23	+07.25 \pm 1.32
	Mode II	−08.68 \pm 1.65	+00.25 \pm 0.73	+01.50 \pm 0.28	+08.37 \pm 0.93

Table 4. Mean GVD values for the two fundamental modes of each of the four elliptical-core PM-ZBLAN fibres at selected wavelengths, with their corresponding measurement error $\pm 4 \times$ standard deviation.

For the GVD measurements, a similar error analysis was performed. For each fundamental mode of each fibre, three measurements were performed by varying the phase-matching point. The standard deviation between these three measurements

was calculated to quantify the experimental uncertainty.

The systematic uncertainty in the fibre length of ± 1 mm was also incorporated. This systematic error was then combined with the standard deviation from the three independent measurements using the root-sum-of-squares approach to determine the total uncertainty. A representative GVD curve is shown in blue in Fig. 3(e)–(h), with the corresponding error band of $\pm 4 \times$ standard deviation shown in shades of orange. The mean GVD at selected wavelengths for both the fundamental modes of each of the fibres is provided in Table 4, with a corresponding measurement error of $\pm 4 \times$ standard deviation. The factor of $\pm 4 \times$ the standard deviation of the GVD measurements was chosen, rather than $\pm 2 \times$, primarily to ensure that the error band is clearly visible in the plots.

Data and code availability

The wavelength versus mean group birefringence for the four elliptical-core PM-ZBLAN fibres is available through Figshare³⁴. The group velocity dispersion, which can be obtained by substituting the A-coefficients provided in Table 2 into Eq. (3) for both fundamental modes of the four elliptical-core PM-ZBLAN fibres, is also available through Figshare³⁴. Standard software packages were used for all analyses. No additional code is available.

Acknowledgements

The authors thank FiberLabs Inc., Japan, for providing the ZBLAN fibre samples and data in Table 1.

Funding

Danmarks Frie Forskningsfond project no. 2031-00009B; VILLUM Fonden (2021 Villum Investigator project no. 00037822: Table-Top Synchrotrons); Innovation Fund Denmark project no. 2105-00039B (HYPERSORT); EU's Horizon Europe project no. 101058054 (TURBO); Schweizerischer Nationalfonds zur Förderung der Wissenschaftlichen Forschung (TMPFP2_210543, PCEFP2_181222).

References

1. Agrawal, G. P. *Nonlinear Fiber Optics* (Academic Press, 2019), 6 edn. [10.1016/C2018-0-01168-8](https://doi.org/10.1016/C2018-0-01168-8).
2. Dudley, J. M. & Taylor, J. R. *Supercontinuum generation in optical fibers* (Cambridge University Press, 2010), 1 edn. [10.1017/CBO9780511750465](https://doi.org/10.1017/CBO9780511750465).
3. Islam, M. N., Sucha, G., Bar-Joseph, I., Wegener, M., Gordon, J. P. & Chemla, D. S. Broad bandwidths from frequency-shifting solitons in fibers. *Optics Letters* **14.7**, 370–372, [10.1364/OL.14.000370](https://doi.org/10.1364/OL.14.000370) (Apr. 1989).
4. Wadsworth, W. J., Joly, N., Knight, J. C., Birks, T. A., Biancalana, F. & Russell, P. S. J. Supercontinuum and four-wave mixing with q-switched pulses in endlessly single-mode photonic crystal fibres. *Optics Express* **12.2**, 299–309, [10.1364/OPEX.12.000299](https://doi.org/10.1364/OPEX.12.000299) (Jan. 2004).
5. McConnell, G., Girkin, J. M., Ameer-Beg, S. M., Barber, P. R., Vojnovic, B., Ng, T., Banerjee, A., Watson, T. F. & Cook, R. J. Time-correlated single-photon counting fluorescence lifetime confocal imaging of decayed and sound dental structures with a white-light supercontinuum source. *Journal of Microscopy* **225.2**, 126–136, [10.1111/j.1365-2818.2007.01724.x](https://doi.org/10.1111/j.1365-2818.2007.01724.x) (Feb. 2007).
6. Jalink, K., Diaspro, A., Corsi, V., Bianchini, P., Borlinghaus, R. & Young, S. The first supercontinuum confocal that adapts to the sample (2008). Leica reSearch Newsletter, Accessed: 2025-05-19.
7. Nakazawa, M., Tamura, K., Kubota, H. & Yoshida, E. Coherence degradation in the process of supercontinuum generation in an optical fiber. *Optical Fiber Technology* **4.2**, 215–223, [10.1006/ofte.1998.0253](https://doi.org/10.1006/ofte.1998.0253) (Apr. 1998).
8. Dudley, J. M., Genty, G. & Coen, S. Supercontinuum generation in photonic crystal fiber. *Rev. Mod. Phys.* **78**, 1135–1184, [10.1103/RevModPhys.78.1135](https://doi.org/10.1103/RevModPhys.78.1135) (Oct. 2006).
9. Heidt, A. M. Pulse preserving flat-top supercontinuum generation in all-normal dispersion photonic crystal fibers. *Journal of the Optical Society of America B* **27.3**, 550–559, [10.1364/JOSAB.27.000550](https://doi.org/10.1364/JOSAB.27.000550) (Mar. 2010).
10. Klimczak, M., Soboń, G., Kasztelanic, R., Abramski, K. M. & Buczyński, R. Direct comparison of shot-to-shot noise performance of all normal dispersion and anomalous dispersion supercontinuum pumped with sub-picosecond pulse fiber-based laser. *Scientific Reports* **6**, 1–14, [10.1038/srep19284](https://doi.org/10.1038/srep19284) (Jan. 2016).

11. Rao D. S., S., Engelholm, R. D., Gonzalo, I. B., Zhou, B., Bowen, P., Moselund, P. M., Bang, O. & Bache, M. Ultra-low-noise supercontinuum generation with a flat near-zero normal dispersion fiber. *Optics Letters* **44.9**, 2216–2219, [10.1364/OL.44.002216](https://doi.org/10.1364/OL.44.002216) (May. 2019).
12. Bravo Gonzalo, I., Engelholm, R. D., Sørensen, M. P. & Bang, O. Polarization noise places severe constraints on coherence of all-normal dispersion femtosecond supercontinuum generation. *Scientific Reports* **8.6579**, 1–13, [10.1038/s41598-018-24691-7](https://doi.org/10.1038/s41598-018-24691-7) (Apr. 2018).
13. Brainis, E., Amans, D. & Massar, S. Scalar and vector modulation instabilities induced by vacuum fluctuations in fibers: Numerical study. *Physical Review A* **71.2**, 023808–1–023808–13, [10.1103/PhysRevA.71.023808](https://doi.org/10.1103/PhysRevA.71.023808) (Feb. 2005).
14. Rao D. S., S., Karpate, T., Ghosh, A. N., Gonzalo, I. B., Klimczak, M., Pysz, D., Buczyński, R., Billet, C., Bang, O., Dudley, J. M. & Sylvestre, T. Noise in supercontinuum generated using pm and non-pm tellurite glass all-normal dispersion fibers. *Optics Letters* **47.10**, 2550–2553, [10.1364/OL.455571](https://doi.org/10.1364/OL.455571) (May. 2022).
15. Genier, E., Grelet, S., Engelholm, R. D., Bowen, P., Moselund, P. M., Bang, O., Dudley, J. M. & Sylvestre, T. Ultra-flat, low-noise, and linearly polarized fiber supercontinuum source covering 670–1390 nm. *Optics Letters* **46.8**, 1820–1823, [10.1364/OL.420676](https://doi.org/10.1364/OL.420676) (Apr. 2021).
16. Sierro, B., Hänzi, P., Spangenberg, D., Rampur, A. & Heidt, A. M. Reducing the noise of fiber supercontinuum sources to its limits by exploiting cascaded soliton and wave breaking nonlinear dynamics. *Optica* **9.4**, 352–359, [10.1364/OPTICA.450505](https://doi.org/10.1364/OPTICA.450505) (Mar. 2022).
17. Heidt, A. M., Rothhardt, J., Hartung, A., Bartelt, H., Rohwer, E. G., Limpert, J. & Tünnermann, A. High quality sub-two cycle pulses from compression of supercontinuum generated in all-normal dispersion photonic crystal fiber. *Optics Express* **19.15**, 13873–13879, [10.1364/OE.19.013873](https://doi.org/10.1364/OE.19.013873) (Jul. 2011).
18. Liu, Y., King, M. D., Tu, H., Zhao, Y. & Boppart, S. A. Broadband nonlinear vibrational spectroscopy by shaping a coherent fiber supercontinuum. *Optics Express* **21.7**, 8269–8275, [10.1364/OE.21.008269](https://doi.org/10.1364/OE.21.008269) (Apr. 2013).
19. Rao D. S., S., Jensen, M., Grüner-Nielsen, L., Olsen, J. T., Heiduschka, P., Kemper, B., Schnekenburger, J., Glud, M., Mogensen, M., Israelsen, N. M. & Bang, O. Shot-noise limited, supercontinuum-based optical coherence tomography. *Light: Science & Applications* **10.1**, 1–13, [10.1038/s41377-021-00574-x](https://doi.org/10.1038/s41377-021-00574-x) (Jun. 2021).
20. Kaltenecker, K. J., Rao D. S., S., Rasmussen, M., Lassen, H. B., Kelleher, E. J. R., Krauss, E., Hecht, B., Mortensen, N. A., Grüner-Nielsen, L., Markos, C., Bang, O., Stenger, N. & Jepsen, P. U. Near-infrared nanospectroscopy using a low-noise supercontinuum source. *APL Photonics* **6.6**, 066106–1–10, [10.1063/5.0050446](https://doi.org/10.1063/5.0050446) (Jun. 2021).
21. Gruber, C., Pupeikis, J., Camenzind, S. L., Willenberg, B., Camargo, F. V. A., Lang, L., Hamm, P., Rampur, A., Heidt, A., Phillips, C. R., Cerullo, G. & Keller, U. High-sensitivity pump-probe spectroscopy with a dual-comb laser and a pm-andi supercontinuum. *Optics Letters* **49.22**, 6445–6448, [10.1364/OL.538105](https://doi.org/10.1364/OL.538105) (Nov. 2024).
22. Israelsen, N. M., Petersen, C. R., Barh, A., Jain, D., Jensen, M., Hannesschläger, G., Tidemand-Lichtenberg, P., Pedersen, C., Podoleanu, A. & Bang, O. Real-time high-resolution mid-infrared optical coherence tomography. *Light: Science & Applications* **8.11**, 1–13, [10.1038/s41377-019-0122-5](https://doi.org/10.1038/s41377-019-0122-5) (Jan. 2019).
23. Hagen, C., Walewski, J. & Sanders, S. Generation of a continuum extending to the midinfrared by pumping zblan fiber with an ultrafast 1550-nm source. *IEEE Photonics Technology Letters* **18.1**, 91–93, [10.1109/LPT.2005.860390](https://doi.org/10.1109/LPT.2005.860390) (Jan. 2006).
24. Xia, C., Kumar, M., Kulkarni, O. P., Islam, M. N., Fred L. Terry, J., Freeman, M. J., Poulain, M. & Mazé, G. Mid-infrared supercontinuum generation to 4.5 μm in zblan fluoride fibers by nanosecond diode pumping. *Optics Letters* **31.17**, 2553–2555, [10.1364/OL.31.002553](https://doi.org/10.1364/OL.31.002553) (09. 2006).
25. Plyler, E. K., Jr., H. C. A. & Tidwell, E. D. Emission spectrum of carbon monoxide from 2.3 to 2.5 microns. *Journal of Research of the National Bureau of Standards* **61.1**, 53–57 (Jul. 1958). Research Paper 2883.
26. Plyler, E. K. & Blaine, L. R. Infrared emission spectrum of methane at 3.3 microns. *Journal of Research of the National Bureau of Standards* **59.5**, 317–318 (Nov. 1957). Research Paper 2803.
27. Benedict, W. S., Plyler, E. K. & Tidwell, E. D. Vibration–rotation bands of ammonia: 1. the combination bands $v_2 + (v_1, v_3)$. *Journal of Research of the National Bureau of Standards* **61.3**, 123–147 (Sep. 1958). Research Paper 2894.
28. Gao, W., Ogawa, K., Xue, X., Liao, M., Deng, D., Cheng, T., Suzuki, T. & Ohishi, Y. Third-harmonic generation in an elliptical-core zblan fluoride fiber. *Optics Letters* **38.14**, 2566–2568, [10.1364/OL.38.002566](https://doi.org/10.1364/OL.38.002566) (Jul. 2013).
29. Yanagita, H., Masuda, I., Yamashita, T. & Toratani, H. Diode laser pumped er^{3+} fibre laser operation between 2.7–2.8 μm . *Electronics Letters* **26**, 1836–1838, [10.1049/el:19901182](https://doi.org/10.1049/el:19901182) (Oct. 1990).

30. Fresnel, A.-J. *Mémoire sur la double réfraction que la lumière éprouve en traversant les aiguilles de quartz suivant les directions parallèles à l'axe*, vol. 2 (Imprimerie Impériale, 1866). Originally presented in 1822.
31. Rashleigh, S. C. Wavelength dependence of birefringence in highly birefringent fibers. *Optics letters* **7.6**, 294–296, [10.1364/OL.7.000294](https://doi.org/10.1364/OL.7.000294) (Jun. 1982).
32. Mueller, D., West, J. A. & Koch, K. W. Interferometric chromatic dispersion measurement of a photonic band-gap fiber. In Dutta, A. K., Awwal, A. A. S., Dutta, N. K. & Okamoto, K. (eds.) *Active and Passive Optical Components for WDM Communications II*, vol. 4870, 446–454, [10.1117/12.475553](https://doi.org/10.1117/12.475553) (SPIE, Jun. 2002).
33. Hlubina, P., Kadulová, M. & Ciprian, D. Spectral interferometry-based chromatic dispersion measurement of fibre including the zero-dispersion wavelength. *Journal of the European Optical Society - Rapid Publications* **7**, 12017, [10.2971/jeos.2012.12017](https://doi.org/10.2971/jeos.2012.12017) (Oct. 2012).
34. Rao D. S., S., Petersen, C. R., Rampur, A., Bang, O. & Heidt, A. M. Dataset for 'Measured group birefringence and group velocity dispersion of elliptical-core ZBLAN fibres for mid-infrared supercontinuum generation'. *Figshare*, [10.6084/m9.figshare.c.8226784](https://doi.org/10.6084/m9.figshare.c.8226784) (Jan. 2026).
35. Rao D. S., S. Ph.D. thesis. *Low-noise supercontinuum sources utilizing normally dispersive fibers* (Apr. 2020). URL <https://orbit.dtu.dk/en/publications/low-noise-supercontinuum-sources-utilizing-normally-dispersive-fi>.
36. Kubat, I., Agger, C. S., Moselund, P. M. & Bang, O. Mid-infrared supercontinuum generation to 4.5 μm in uniform and tapered zblan step-index fibers by direct pumping at 1064 or 1550 nm. *Journal of the Optical Society of America B* **30.10**, 2743–2757, [10.1364/JOSAB.30.002743](https://doi.org/10.1364/JOSAB.30.002743) (Oct. 2013).
37. Folkenberg, J., Nielsen, M., Mortensen, N., Jakobsen, C. & Simonsen, H. Polarization maintaining large mode area photonic crystal fiber. *Optics Express* **12.5**, 956–960, [10.1364/OPEX.12.000956](https://doi.org/10.1364/OPEX.12.000956) (Mar. 2004).
38. Ciąćka, P., Rampur, A., Heidt, A., Feurer, T. & Klimczak, M. Dispersion measurement of ultra-high numerical aperture fibers covering thulium, holmium, and erbium emission wavelengths. *Journal of the Optical Society of America B* **35.6**, 1301–1307, [10.1364/JOSAB.35.001301](https://doi.org/10.1364/JOSAB.35.001301) (Jun. 2018).
39. Petersen, C. R., Møller, U., Kubat, I., Zhou, B., Dupont, S., Ramsay, J., Benson, T., Sujekci, S., Abdel-Moneim, N., Tang, Z., Furniss, D., Seddon, A. & Bang, O. Mid-infrared supercontinuum covering the 1.4–13.3 μm molecular fingerprint region using ultra-high na chalcogenide step-index fibre. *Nature Photonics* **8.11**, 830–834, [10.1038/nphoton.2014.213](https://doi.org/10.1038/nphoton.2014.213) (Nov. 2014).
40. Demetriou, G., Bérubé, J.-P., Vallée, R., Messaddeq, Y., Petersen, C. R., Jain, D., Bang, O., Craig, C., Hewak, D. W. & Kar, A. K. Refractive index and dispersion control of ultrafast laser inscribed waveguides in gallium lanthanum sulphide for near and mid-infrared applications. *Optics Express* **24.6**, 6350–6358, [10.1364/OE.24.006350](https://doi.org/10.1364/OE.24.006350) (Mar. 2016).

Author contributions

S.R.D.S. and C.R.P. designed, and set up the group birefringence and dispersion measurement system. S.R.D.S. performed the experiments. S.R.D.S., A.R., and C.R.P. carried out the data processing and analysis. O.B. and A.M. oversaw the experimental work. All authors participated in the planning, drafting, and revision of the manuscript.

Competing interests

The authors declare no competing interests.

Additional information

Correspondence and requests for materials should be addressed to S.R.D.S.

© The Author(s) 2025